10.4 Synthesis of MFe_2O_4 nanoparticles by the Oil-in-Water microemulsion reaction method and its exploration for photocatalytic water splitting

Arturo Adrián Rodríguez Rodríguez, Maira Berenice Moreno Trejo, Miguel de Jesús Meléndez Zaragoza, Virginia Collins Martínez, Alejandro López Ortíz, Eduardo Martínez Guerra, Margarita Sánchez Domínguez.

[1] Centro de Investigación en Materiales Avanzados, S. C. (CIMAV), Unidad Monterrey, Alianza Norte 202, Parque de Investigación e Innovación Tecnológica, 66628 Apodaca, México.

[2] CIMAV Unidad Chihuahua, Av. Miguel de Cervantes Saavedra 120, Complejo Industrial Chihuahua, 31136 Chihuahua, Chih. México.

* Corresponding author: (+52) 8448073209, arturo.rodriguez@cimav.edu.mx, margarita.sanchez@cimav.edu.mx

ABSTRACT

Spinel-type ferrites have the molecular formula MFe_2O_4, where M represents a divalent metallic cation, such as Co^{2+}, Ni^{2+} and Zn^{2+} for $CoFe_2O_4$, $NiFe_2O_4$ and $ZnFe_2O_4$, respectively. As photocatalyst, spinel-type ferrites have shown an efficient visible light absorption, high sorption capacity, thermal stability, and low toxicity. Moreover its magnetic response allows their easy recovery from the liquid reaction media. Thanks to these features, MFe_2O_4 compounds are a promising option for the photocatalytic water-splitting, a clean and simple technology to obtain H_2, which has not been fully explored for MFe_2O_4 nanoparticles, especially those synthesized by microemulsion. In light of this, we prepared cobalt, nickel and zinc ferrites employing the novel oil-in-water microemulsion reaction method and explored its H_2 evolution through water splitting reaction. In order to perform the photocatalytic experiments, a dispersion of nanoparticles in water (2% MeOH) was prepared inside a quartz tube reactor; this system was sealed, and then illuminated with a 250 W white mercurial lamp. H_2 production was monitored by gas chromatography. Prior to photocatalytic evaluation, as-synthesized nanomaterials were thermally treated and characterized. Characterization results showed globular nanoparticles with a cubic spinel-type crystalline structure, adequate textural properties for photocatalytic applications and UV-visible light absorption. In regard to light-driven H_2 production, the photoactivity of these oxides was successfully demonstrated; photocatalytic water splitting evaluation of $ZnFe_2O_4$ yielded a higher amount of hydrogen (354 $\mu molH_2g^{-1}$) compared with Co^{2+} and Ni^{2+} ferrites in an 8 h experiment. Broadly, this work represents a new contribution to the studies of spinel-type ferrites for the photocatalytic production of H_2.

Keywords: ferrites nanoparticles; oil-in-water microemulsion; H_2 production; photocatalytic water-splitting

1. Introduction

Nowadays, owing the search of alternative and green energy sources, molecular hydrogen (H_2) has become a strong candidate to replace fossil fuels. As a consequence, the implementation of clean technologies, as the photocatalytic splitting of water molecule, are being envisaged as promising techniques to produce H_2. [1-3] The photocatalytic water splitting involves the use of a powder photocatalyst, well-dispersed in water (usually with a sacrificial agent as methanol), and contained in a sealed reactor, irradiated by a photon energy source. The photocatalyst, generally an inorganic semiconductor material, must meet the energetic requirements for either reduction of protons (H^+ / H_2, 0 V vs NHE a pH=0) and/or oxidation of water (O_2 / H_2O, 1.23 V vs NHE pH=0), in order to provoque the splitting of H_2O molecule into H_2 and ½ O.[4-7] Several types of inorganic nanomaterials have been studied for photocatalytic water splitting [8-13], among them spinel-type ferrites nanoparticles have gained great interest due its remarkable properties [14-16]. Spinel-type ferrites are a group of iron oxides with the molecular formula MFe_2O_4, where M represents a divalent metallic cation, such as Co^{2+}, Ni^{2+} and Zn^{2+}, in the case of cobalt ($CoFe_2O_4$), nickel ($NiFe_2O_4$) and zinc ferrites ($ZnFe_2O_4$). As photocatalyst, $CoFe_2O_4$, $NiFe_2O_4$ and $ZnFe_2O_4$ nanoparticles have shown an efficient visible light absorption (which promotes the photocatalytic redox reactions) due its relative low bandgaps (<2 eV), good electrical conductivity (favorable for the transfer of electrons and holes), high molecular adsorption-desorption capability, stability against photocorrosion, low toxicity, and easy and low cost preparation; moreover its magnetic response (moderate magnetic saturation, and low magnetic remanence) allows to recover them from the liquid reaction media, by the application of an external magnetic field [17-20]. Although the increasing interest of spinel-type ferrites in regard photocatalytic production of H_2, the capacity of this family of iron oxides has not been fully explored yet, especially with MFe_2O_4 nanoparticles synthesized by microemulsion methods such as the oil-in-water (O/W) microemulsion reaction method, which has been used recently to synthesize photocatalyst nanoparticles for the degradation of water pollutants [21, 22]. Roughly, the O/W microemulsion reaction method consist in the use of oil droplets (2-50 nm), in which organometallic precursors are dissolved, stabilized by a surfactant, and dispersed in a continuous aqueous phase. When a precipitating agent is added, the reagents will contact each other at the interface, and they will react to form precipitates of nanometric size, the nanoparticles. The benefits of using this method are mainly the possibility to obtain very small particles with good textural properties and homogeneous composition at mild conditions. More information about the O/W microemulsion reaction method can be found in our previous works. [23, 24] In this context, the present work represents a new contribution to the studies of $CoFe_2O_4$

$NiFe_2O_4$, and $ZnFe_2O_4$ spinel-type ferrites, for the light driven production of H_2 by water splitting reaction. Detailed characterization of prepared and thermal treated nanoparticles, in terms of structure, morphology, textural and optical properties were a valuable tool to the understanding of spinel-type ferrites photocatalytic activity.

2. Materials and Methods

2.1 Materials

2.1.1 MFe_2O_4 (M: Co^{2+}, Ni^{2+} and Zn^{2+}) nanoparticles synthesis

Iron (III) 2-ethylhexanoate ($C_{24}H_{45}FeO_6$, nominally 50% in mineral spirits) and zinc (II) 2-ethylhexanoate ($C_{16}H_{30}ZnO_4$, nominally 50% in mineral spirits) were purchased from Alfa Aesar. Cobalt (II) 2-ethylhexanoate ($C_{16}H_{30}CoO_4$, 65 wt% solution in mineral spirits), nickel (II) 2-ethylhexanoate ($C_{16}H_{30}NiO_4$, 78 % in 2-ethylhexanoic acid), isooctane (C_8H_{18}, CHROMASOLV® Plus for HPLC, $\geq$ 99.5%), tetramethylammonium hydroxide pentahydrate TMAH ($C_4H_{13}NO{\cdot}5H_2O$, $\geq$ 97 %) were purchased from Sigma-Aldrich. Synperonic^{TM} 91/5 ($C_{19}O_6H_{40}$) was purchased from CRODA.

2.1.2 Photocatalytic water splitting evaluation

Distilled water (H_2O) and methanol (CH_4O, HPLC grade) were purchased from J.T. Baker. Ultrapure gaseous nitrogen (N_2: $\geq$ 99.998 %), used as gas carrier for chromatography.

2.2 Methods

2.1 MFe_2O_4 (M: Co^{2+}, Ni^{2+} and Zn^{2+}) nanoparticles synthesis

Three compositions of spinel-type ferrite nanoparticles were similarly synthesized, employing the oil-in-water microemulsion reaction method. For this purpose an oil/surfactant/deionized water pseudo-ternary system, with a 20/20/60 weight percent ratio (wt %) composition, was prepared. Isooctane was used as oil, in which Fe (III) 2-EH, and Co (II) 2-EH; for $CoFe_2O_4$, or Ni (II) 2-ethylhexanoate; for $NiFe_2O_4$, or Zn (II) 2-ethylhexanoate; for $ZnFe_2O_4$, in stoichiometric proportions (M:Fe 1:2), were previously dissolved, and further incorporated to the surfactant and deionized water. As surface active agent, synperonic^{TM} 91/5 was employed. Pseudo-ternary system constituents were properly weighted on glass vessels, closed and then placed in a water bath with controlled temperature and magnetic stirring. Raising-up temperature close to 40 °C, led to the

corresponding oil-in-water microemulsion formation, as depicted by the apparition of dark-brown translucent solutions. The O/W microemulsion reactions were carried out at 46 °C; in the case of cobalt ferrite, and 41 °C and 40 °C; in the case of nickel and zinc ferrites respectively, by continuous addition of a 1 M TMAH solution (under magnetic stirring) until reaching a pH of 12-12.45. Nanoparticles presence was indicated by the formation of a dark solid. Magnetic stirring and temperature conditions were maintained for 24 hours. The obtained solids were washed several times with water (until neutral pH was achieved), isopropanol and chloroform, to remove by-products. Finally, products were dried at 70 °C for 24 hours, and thermally treated at 500 °C for 5 hours.

2.3 MFe_2O_4 (M: Co^{2+}, Ni^{2+} and Zn^{2+}) nanoparticles characterization

Crystalline phases of as-prepared and thermally treated MFe_2O_4 nanoparticles were identified by X-ray diffraction (XRD), on a PANalytical Empyrean diffractometer with CuK_α radiation; diffractograms were recorded with a step size of 0.0167113° and a time per step of 59.69 s. The morphology of thermal treated nanoparticles was studied by high-resolution transmission electron microscopy in scanning mode (HRTEM-STEM), employing a field emission transmission electron microscope JEM-2200FS, operated at 200 kV. Textural properties were determined by nitrogen adsorption–desorption isotherms (at 77 K), employing an automatic Quantachrome Autosorb instrument; prior to N_2 adsorption, all the samples were outgassed. Specific surface area was calculated using the Brunauer-Emmet-Teller (BET) method. Optical properties were determined by diffuse reflectance (DR) UV-Vis measurements, using an UV-Vis-NIR spectrophotometer from Perkin Elmer, with an integrating sphere configuration.

2.3 Photocatalytic water splitting

In order to perform photocatalytic water splitting experiments, a dispersion of MFe_2O_4 nanoparticles (200 mg) in 200 mL of water (with a 2% of methanol, MeOH) was prepared inside a quartz tube reactor (photoreactor); this system was closed by two aluminum flanges bolted together by threaded rods, and properly sealed to avoid gas leaks. Photoreactor was then illuminated with a white mercurial lamp of 250 Watts (Philips MH/U 250W/640). H_2 evolution was monitored hourly (for 8 h) by a Clarus 580 Perkin Elmer gas chromatograph equipped with a thermal conductivity detector. Evolved gas sampling was carried out through a septum port located on the top of the photoreactor, and then transferred to the chromatograph (1 mL) by injection using a precision analytical syringe (VICI precision sampling, inc.) for gases.

3. Results and Discussion

3.1 MFe_2O_4 (M: Co^{2+}, Ni^{2+} and Zn^{2+}) nanoparticles characterization

3.1.1 X-ray diffraction (XRD)

Fig. 1 (left) shows the XRD patterns of as-obtained (Co^{2+}, Ni^{2+} and Zn^{2+}) ferrites. First, as it can be seen $CoFe_2O_4$ pattern displays typical peaks of a polycrystalline material, whose positions and relative intensities at specific 2Θ (°) values can be matched with the (111), (220), (311), (400), (511), and (440) crystalline planes of cubic spinel-type cobalt ferrite (*, JCPDS 04-006-4150). Secondly, $ZnFe_2O_4$ ferrite pattern shows a more broadened and less defined profile compared with Co^{2+} composition; however, it is still possible to identify the main cubic MFe_2O_4 spinel-type peaks, matched with the (220), (311), (400), (511), and (440) crystalline planes. Finally, $NiFe_2O_4$ shows the broadest and low intensity peaks among synthesized ferrites, even though it also displays the (311), (400) and (440) crystalline planes related to spinel-type structure. Broadly, the depicted diffractograms have a typical profile for nanoparticles. After treating the as-obtained materials at 500 °C for 5h (fig. 1, right), the samples patterns clearly revealed sharper profiles and an increment of crystalline peaks, indicating an enhanced crystallinity as a result of the atomic ordering promoted by thermal treatment. The identified signals confirm again the formation of pure cobalt ferrite, as well as the nickel (+, ICDD 00-044-1485) and zinc cubic spinel-type structures (∧, ICSD 98-011-6750). Comparing the (Co^{2+}, Ni^{2+} and Zn^{2+}) ferrites patterns, it is possible to observe slight displacements in main crystalline planes, in part due the ionic radii of divalent metals (Zn^{2+}: 0.88 Å = Co^{2+}: 0.838 Å > Ni^{2+}: 0.731 Å [25]) that composes the crystalline $M^{2+}Fe_2O_4$ structure. Based on experimental and reference diffractograms, Rietveld refinement was performed to estimate the crystallite mean size (d_{XRD}) and lattice parameter of prepared ferrites. In regard obtained values, $ZnFe_2O_4$ has the higher d_{XRD}: 10 nm, followed by $CoFe_2O_4$ ferrite d_{XRD}: 8 nm and $NiFe_2O_4$ d_{XRD}: 4 nm. Calculated lattice parameter values ($ZnFe_2O_4$: 8.4370 Å, $CoFe_2O_4$: 8.3961, $NiFe_2O_4$: 8.3393 Å) are in agreement with the reported for identified crystalline phases ($ZnFe_2O_4$: 8.4379 Å, $CoFe_2O_4$: 8.3961 Å, $NiFe_2O_4$: 8.3393 Å). XRD results probes the capacity of the O/W microemulsion method to produce semicrystalline (Co^{2+}, Zn^{2+}, Ni^{2+})Fe_2O_4 ferrites at mild conditions using TMAH 1M solution as precipitation agent, and although a thermal treatment is needed to enhance nanomaterials crystallinity, the employed conditions are not as high as commonly needed in other synthesis methods [26, 27].

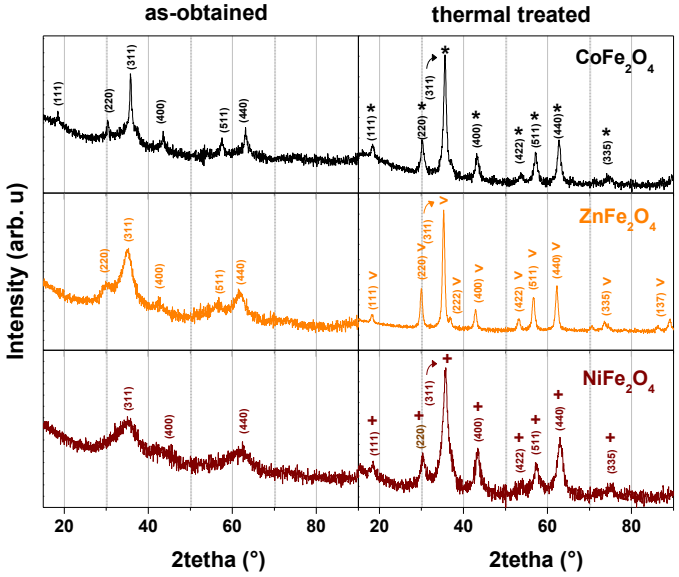

Fig. 1. X-Ray diffraction patterns of $(Co^{2+}, Zn^{2+}, Ni^{2+})Fe_2O_4$ nanoparticles: before (as-obtained) and after thermal treatment.

3.1.2 High-resolution transmission electron microscopy in scanning mode (HRTEM-STEM)

Fig. 2 displays bright field HRTEM-STEM electron micrographs of thermally treated nanoparticles: (a) cobalt, (b) nickel and (c) zinc ferrites. As evident, $CoFe_2O_4$ analyzed zone shows agglomerated globular nanoparticles, with sizes around 20 nm; similarly, $NiFe_2O_4$ and $ZnFe_2O_4$ micrographs exhibits agglomerated globular nanoparticles but with smaller sizes (around 14 nm) and apparently a more defined morphology. Cobalt ferrite nanoparticles are larger since, as evidenced by XRD, the $CoFe_2O_4$ crystalline phase was already formed before thermal treatment (in comparison with nickel and zinc ferrites), and thus when the samples were treated at 500 °C for 5 h, the growth of nanoparticles was more favored. Corresponding inset images display nanocrystals, which composes ferrite nanoparticles. The observed lattice fringes makes evident the crystallinity of prepared MFe_2O_4 structures; the measured interplanar spacings ($CoFe_2O_4$ (022) = ~ 2.9 Å, $NiFe_2O_4$ (111) = ~ 4.8 Å and $ZnFe_2O_4$ (311) = ~ 2.5 Å) are in good accordance with cubic-spinel phases of cobalt (JCPDS 04-006-4150), nickel (ICDD 00-044-1485) and zinc (ICSD 98-011-6750) ferrites. As demonstrated, HRTEM-STEM results confirms the successful formation of crystalline ferrite nanoparticles using the employed preparation method.

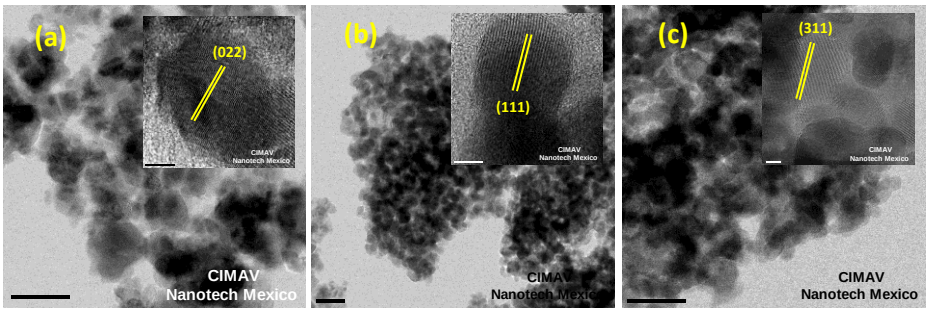

Fig. 2. HRTEM-STEM images of thermal treated samples: (a) $CoFe_2O_4$, (b) $NiFe_2O_4$ and (c) $ZnFe_2O_4$.

3.1.3 Textural properties

N_2 adsorption/desorption isotherm curves of thermal treated (Co^{2+}, Ni^{2+} and Zn^{2+})Fe_2O_4 nanoparticles are presented on fig. 3. In the case of cobalt ferrite, the gas sorption measuring depicts a type-IV curve (IUPAC classification), with a hysteresis loop characteristic of a presumably mesoporous material (pore sizes between 2-50 nm) in the 0.6-1 range of relative pressure [28]. Similarly, nickel and zinc ferrites sorption processes exhibit type-IV curves (with hysteresis loops), but with an apparently higher amount of N_2 sorption than cobalt ferrite, and in a distinct relative pressure scale. These differences can be associated to the texture of prepared nanoparticles, as well to the peculiar interparticle arrangements of each system, achieved from packing of neighbouring nanoparticles (observed by HRTEM-STEM). Additionally, specific surface areas (SSA) were calculated by BET method, values of 63.823 m^2/g, 64.699 m^2/g and 49.311 m^2/g were obtained for Co^{2+}, Ni^{2+}, and Zn^{2+} ferrites, respectively. Obtained textural properties demonstrate the capacity of the O/W microemulsion to produce materials with adequate surface areas and sorption capability for catalytic applications.

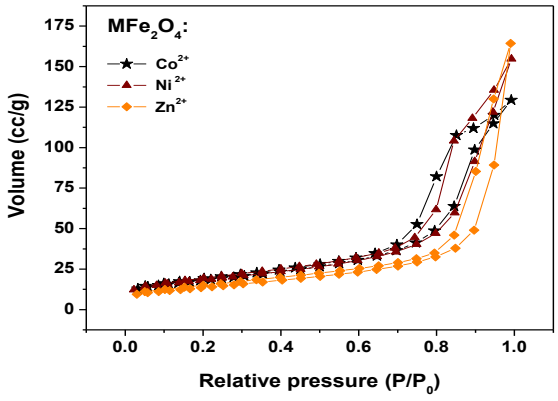

Fig. 3. N_2 adsorption/desorption isotherms of thermal treated (Co^{2+}, Zn^{2+}, Ni^{2+})Fe_2O_4 nanoparticles.

3.1.4 Diffuse Reflectance UV-Vis spectroscopy (DR UV-Vis)

In fig. 4a the absorbance spectra of thermally treated (Co^{2+}, Ni^{2+} and Zn^{2+})Fe_2O_4 nanoparticles, measured by diffuse reflectance UV-Vis experiments, are presented. The broader spectra corresponds to the $CoFe_2O_4$ nanoparticles, and as it can be inferred, this material strongly absorbs photons from UV and visible-light region. In comparison, $NiFe_2O_4$ and $ZnFe_2O_4$ nanoparticles spectras exhibit also UV- visible light absorption, but within a shorter visible-light range, as depicted in an absorption decrement in the 500-700 nm wavelength. Moreover, in the case of nickel ferrite spectra it is possible to observe a shoulder-type band around 750 nm, which according to other works is typical of $NiFe_2O_4$, and it can be attributed to the d–d transition from Ni3d-t_{2g} to Ni3d-e_g [29]. To the best of our knowledge, this band has not been reported for Co^{2+} and Zn^{2+} compositions. The light absorption properties of thermally treated MFe_2O_4 nanoparticles, is related to the presence of Co^{2+}, Ni^{2+} or Zn^{2+} cations in the cubic spinel-type crystalline structure, which implies structural changes (as demonstrated by XRD results), and thus different electronic band structures. The latter, can be assumed due to the estimated optical bandgap energies (Eg): ~1.39 eV for $CoFe_2O_4$, ~1.9 eV for $ZnFe_2O_4$, and ~1.79 eV for $NiFe_2O_4$, calculated by the Tauc method, employing the UV-Vis diffuse reflectance data and considering an indirect transition (F(R)*hv^2, fig. 4b). According to the estimated Eg values, the three spinel-type ferrite nanoparticles possess appropriate forbidden band energies for photocatalytic water splitting (driven by UV or visible light), which requires a minimum theoretical band gap of 1.23 eV [6]. Obtained values are also in accordance with the reported for $CoFe_2O_4$, $NiFe_2O_4$ and $ZnFe_2O_4$ phases [17, 27, 29-31].

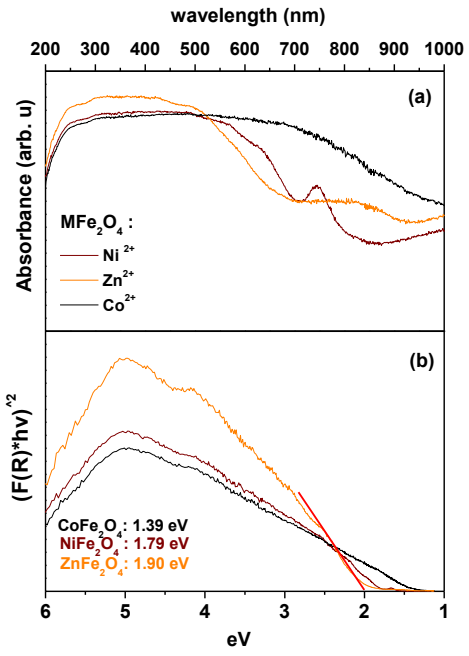

Fig. 4. (a) DR UV-Vis absorption spectra of thermal treated (Co^{2+}, Zn^{2+}, Ni^{2+})Fe_2O_4 nanoparticles, and corresponding (b) Tauc plots for Eg determination.

3.2 MFe_2O_4 (M: Co^{2+}, Ni^{2+} and Zn^{2+}) nanoparticles: photocatalytic water splitting

Fig. 5 depicts the H_2 evolution profiles for Co^{2+}, Ni^{2+} and Zn^{2+} ferrites nanoparticles, photoassisted by white mercurial lamp illumination, as a function of time and using MeOH as sacrificial agent. As can be seen, zinc ferrite has a higher performance from the second hour of photocatalytic evaluation, in comparison with cobalt and nickel ferrites, which display a similar performance. After 8 h of illumination $CoFe_2O_4$, $NiFe_2O_4$ and $ZnFe_2O_4$ yielded the following amounts: 128.00 $\mu molH_2/g$, 128.64 $\mu molH_2/g$, and 353.53 $\mu molH_2/g$, respectively. It is possible to assume that Zn^{2+} ferrite superior H_2 production was achieved because a combination of good crystallinity, small particle size, higher sorption ability, and more importantly suitable bandgap and band edges positions (reported to be around +1.65 V and -0.25 V vs NHE [14]). On the other hand, Co^{2+} and Ni^{2+} ferrites similar photoresponse can be ascribed to its resemblance on textural properties. Comparing with previous scientific reports, T. Peng et al. prepared $NiFe_2O_4$ [29] and $ZnFe_2O_4$ [32] , by a 30 h hydrothermal process, followed by a 500 °C thermal treatment. Regarding photocatalytic water splitting evaluation, zinc ferrite produced 237.87 $\mu molH_2/g$, while nickel ferrite only produced 15.45 $\mu molH_2/g$ after 5 h of reaction. As evident, O/W microemulsion synthesized ferrites presented the same trend, being zinc ferrite as better photocatalyst for H_2 production. In the case of cobalt ferrite evaluation, Y. Ortega-López [27] demonstrated an outstanding performance of $CoFe_2O_4$, using co-precipitation (2540 $\mu molH_2/g$) and ball-milling (3490 $\mu molH_2/g$) as preparation methods, and although in the present study a less promising behavior was observed (128 $\mu molH_2/g$), even compared with O/W microemulsion synthesized $ZnFe_2O_4$, it still represents a new contribution to the investigation studies of MFe_2O_4 ferrites as light driven H_2 producers. Based on ferrites behavior at this test, it was confirmed that spinel-type ferrites (using MeOH) meet the needed conditions for carrying electron-hole pair reactions, in order to promote hydrogen ion reduction to H_2, and possibly MeOH oxidation (to be studied). Thus, it also implies that the employed light source provided enough energy to cause charge separation whereupon photoredox reactions took place.

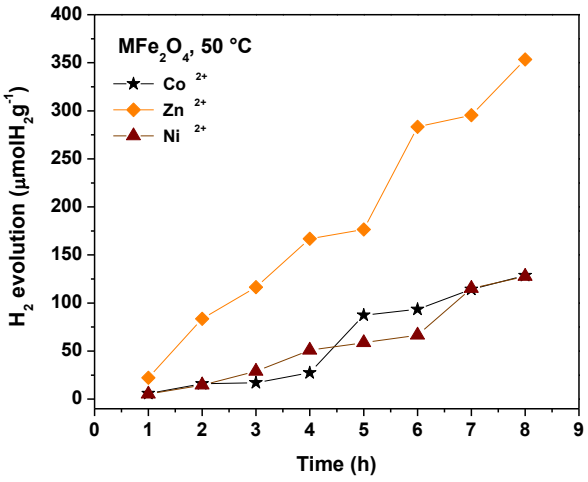

Fig. 5. Hydrogen evolution profile for thermal treated (Co^{2+}, Zn^{2+}, Ni^{2+})Fe_2O_4 nanoparticles in function of time (8 h experiment).

4. Conclusion

In summary, the presented results demonstrated the successful synthesis of globular nanoparticles (< 20 nm) with a cubic MFe_2O_4 (M: Co^{2+}, Ni^{2+} and Zn^{2+}) spinel-type crystalline structure (after thermal treatment) through the feasible oil-in-water microemulsion method. The prepared nanoparticles exhibited textural properties adequate for surface molecular sorption (e.g. H_2O). UV-Vis measurements displayed a good light absorption capability of the spinel-type ferrites, and according to the estimated bandgaps (< 2 eV) these compounds can accomplish both, ultraviolet and visible light absorption. In regard to light-driven H_2 production, the obtained results provided experimental evidence that MFe_2O_4 meet the requirements to reduce protons to generate molecular hydrogen, in the presence of methanol as a sacrificial agent and under white mercurial light illumination. Among the explored compositions, $ZnFe_2O_4$ yielded a higher amount of H_2 compared with Co^{2+} and Ni^{2+} ferrites in an 8 h experiment, due to the combination of its structural, textural and electronic features. The obtained results highlight the usefulness of microemulsion method for the straightforward synthesis of cobalt, nickel and zinc spinel-type ferrites, whose valuable properties can be boosted to the development of novel photocatalysts for water splitting reaction.

Acknowledgements

We are grateful to CONACYT for financial support (CB project grant number CB2011/166649 and Proyecto Redes Temáticas No. 194451). Authors also acknowledge Enrique Longoria (CIMAV Monterrey), Cesar Leyva (CIMAV Chihuahua) and Luis de la Torre Sáenz (CIMAV Chihuahua) for their assistance with XRD, HRTEM-STEM and BET and DR UV-Vis measurements, respectively.

References

[1] T. Jafari, E. Moharreri, A.S. Amin, R. Miao, W. Song, S.L. Suib, Molecules, 21 (2016) 900.
[2] A. López Ortiz, M.J. Meléndez Zaragoza, V. Collins-Martínez, International Journal of Hydrogen Energy, 41 (2016) 23363-23379.
[3] R. Li, Chinese Journal of Catalysis, 38 (2017) 5-12.
[4] H. Ahmad, S.K. Kamarudin, L.J. Minggu, M. Kassim, Renewable and Sustainable Energy Reviews, 43 (2015) 599-610.
[5] K. Maeda, Journal of Photochemistry and Photobiology C: Photochemistry Reviews, 12 (2011) 237-268.
[6] D.J. Martin, Introduction: Fundamentals of Water Splitting and Literature Survey, Investigation into High Efficiency Visible Light Photocatalysts for Water Reduction and Oxidation, Springer International Publishing, Cham, 2015, pp. 1-53.

[7] A.A. Ismail, D.W. Bahnemann, Solar Energy Materials and Solar Cells, 128 (2014) 85-101.
[8] M. Ni, M.K.H. Leung, D.Y.C. Leung, K. Sumathy, Renewable and Sustainable Energy Reviews, 11 (2007) 401-425.
[9] S. Oros-Ruiz, A. Hernández-Gordillo, C. García-Mendoza, A.A. Rodríguez-Rodríguez, R. Gómez, Journal of Chemical Technology & Biotechnology, 91 (2016) 2205-2210.
[10] A. Pérez-Larios, R. Lopez, A. Hernández-Gordillo, F. Tzompantzi, R. Gómez, L.M. Torres-Guerra, Fuel, 100 (2012) 139-143.
[11] Y. Liu, L. Xie, Y. Li, R. Yang, J. Qu, Y. Li, X. Li, Journal of Power Sources, 183 (2008) 701-707.
[12] S. Sun, W. Wang, D. Li, L. Zhang, D. Jiang, ACS Catalysis, 4 (2014) 3498-3503.
[13] C. Zeng, T. Hu, N. Hou, S. Liu, W. Gao, R. Cong, T. Yang, Materials Research Bulletin, 61 (2015) 481-485.
[14] R. Dillert, D.H. Taffa, M. Wark, T. Bredow, D.W. Bahnemann, APL Mater., 3 (2015) 104001.
[15] P.A. Mangrulkar, V. Polshettiwar, N.K. Labhsetwar, R.S. Varma, S.S. Rayalu, Nanoscale, 4 (2012) 5202-5209.
[16] B. Ren, Y. Huang, C. Han, M.N. Nadagouda, D.D. Dionysiou, Ferrites as Photocatalysts for Water Splitting and Degradation of Contaminants, Ferrites and Ferrates: Chemistry and Applications in Sustainable Energy and Environmental Remediation, American Chemical Society, 2016, pp. 79-112.
[17] D. Hong, Y. Yamada, M. Sheehan, S. Shikano, C.-H. Kuo, M. Tian, C.-K. Tsung, S. Fukuzumi, ACS Sustainable Chemistry & Engineering, 2 (2014) 2588-2594.
[18] A. Boudjemaa, I. Popescu, T. Juzsakova, M. Kebir, N. Helaili, K. Bachari, I.-C. Marcu, International Journal of Hydrogen Energy, 41 (2016) 11108-11118.
[19] X. Gao, X. Liu, Z. Zhu, X. Wang, Z. Xie, Scientific Reports, 6 (2016) 30543.
[20] H.M. Gobara, I.M. Nassar, A.M.A. El Naggar, G. Eshaq, Energy, 118 (2017) 1234-1242.
[21] K. Pemartin-Biernath, A. Vela-González, M. Moreno-Trejo, C. Leyva-Porras, I. Castañeda-Reyna, I. Juárez-Ramírez, C. Solans, M. Sánchez-Domínguez, Materials, 9 (2016) 480.
[22] M. Sanchez-Dominguez, G. Morales-Mendoza, M.J. Rodriguez-Vargas, C.C. Ibarra-Malo, A.A. Rodriguez-Rodriguez, A.V. Vela-Gonzalez, S.A. Perez-Garcia, R. Gomez, Journal of Environmental Chemical Engineering, 3 (2015) 3037-3047.
[23] M. Sanchez-Dominguez, M. Boutonnet, C. Solans, Journal of Nanoparticle Research, 11 (2009) 1823-1829.
[24] M. Sanchez-Dominguez, K. Pemartin, M. Boutonnet, Current Opinion in Colloid & Interface Science, 17 (2012) 297-305.
[25] C. Singh, Devika, R. Malik, V. Kumar, S. Singhal, RSC Advances, 5 (2015) 89327-89337.
[26] P. Borse, J. Jang, S. Hong, J.S. Lee, J. Jung, T. Hong, C. Ahn, E. Jeong, K. Hong, J. Yoon, (2009).

[27] Y. Ortega Lopez, H. Medina Vazquez, J. Salinas Gutierrez, V. Guzman Velderrain, A. Lopez Ortiz, V. Collins Martinez, Journal of Nanomaterials, 2015 (2015) 9.
[28] Z.A. ALOthman, Materials, 5 (2012) 2874-2902.
[29] T. Peng, X. Zhang, H. Lv, L. Zan, Catalysis Communications, 28 (2012) 116-119.
[30] R. Dillert, D.H. Taffa, M. Wark, T. Bredow, D.W. Bahnemann, APL Materials, 3 (2015) 104001.
[31] R. Dom, R. Subasri, N.Y. Hebalkar, A.S. Chary, P.H. Borse, RSC Advances, 2 (2012) 12782-12791.
[32] H. Lv, L. Ma, P. Zeng, D. Ke, T. Peng, Journal of Materials Chemistry, 20 (2010) 3665-3672.

[i]Sun, Y., Wu, J., Tian, J., Jin, C., & Yang, R. (2015). Sulfur-doped carbon spheres as efficient metal-free electrocatalysts for oxygen reduction reaction. *ElectrochimicaActa*, *178*, 806-812.

Wang, S., Zhang, L., Xia, Z., Roy, A., Chang, D. W., Baek, J. B., & Dai, L. (2012). BCN graphene as efficient metal-free electrocatalyst for the oxygen reduction reaction. *AngewandteChemie International Edition*, *51*(17), 4209-4212.

[iii]Shui, J., Wang, M., Du, F., & Dai, L. (2015). N-doped carbon nanomaterials are durable catalysts for oxygen reduction reaction in acidic fuel cells. *Science advances*, *1*(1), e1400129.

Wang, S., Dai, C., Li, J., Zhao, L., Ren, Z., Ren, Y., Qui, Y.& Yu, J. (2015). The effect of different nitrogen sources on the electrocatalytic properties of nitrogen-doped electrospun carbon nanofibers for the oxygen reduction reaction. *International Journal of Hydrogen Energy*, *40*(13), 4673-4682.

Zahoor, A., Christy, M., Hwang, Y. J., Lim, Y. R., Kim, P., &Nahm, K. S. (2014). Improved electrocatalytic activity of carbon materials by nitrogen doping. *Applied Catalysis B: Environmental*, *147*, 633-641.

Soo, L. T., Loh, K. S., Mohamad, A. B., Daud, W. R. W., & Wong, W. Y. (2015). An overview of the electrochemical performance of modified graphene used as an electrocatalyst and as a catalyst support in fuel cells. *Applied Catalysis A: General*, *497*, 198-210.

[vii] Wang, S., Zhang, L., Xia, Z., Roy, A., Chang, D. W., Baek, J. B., & Dai, L. (2012). BCN graphene as efficient metal-free electrocatalyst for the oxygen reduction reaction. AngewandteChemie International Edition, 51(17), 4209-4212.

[viii]Yu, L., Pan, X., Cao, X., Hu, P., &Bao, X. (2011). Oxygen reduction reaction mechanism on nitrogen-doped graphene: A density functional theory study. *Journal of catalysis*, *282*(1), 183-190.

[ix]Okamoto, Y. (2009). First-principles molecular dynamics simulation of O 2 reduction on nitrogen-doped carbon. Applied Surface Science, 256(1), 335-341.

[x]Bell, R. P. (2013). The tunnel effect in chemistry. Springer.

[xi]Aquino, N., Campoy, G., &Yee-Madeira, H. (1998). The inversion potential for NH 3 using a DFT approach. *Chemical physics letters*, *296*(1), 111-116.

[xii]Miyasato, T., Kawakami, Y., Kawano, T., &Hiraki, A. (1984). Preparation of sp3-rich amorphous carbon film by hydrogen gas reactive RF-sputtering of graphite, and its properties. Japanese Journal of Applied Physics, 23(4A), L234.

[xiii]Li, Y., Zhang, S., Song, H., Chen, X., Zhou, J., & Hong, S. (2015). New insight into the heteroatom-doped carbon as the electrode material for supercapacitors. *ElectrochimicaActa*, *180*, 879-886.

[xiv]Sanchez-Bojorge, N. A., Rodriguez-Valdez, L. M., Glossman-Mitnik, D., & Flores-Holguin, N. (2015). Theoretical calculation of the maximum absorption wavelength for Cyanidin molecules with several methodologies. *Computational and Theoretical Chemistry*, *1067*, 129-134.

[xv]Hernández-Paredes, J., Glossman-Mitnik, D., Duarte-Moller, A., & Flores-Holguín, N. (2009). Theoretical calculations of molecular dipole moment, polarizability, and first hyperpolarizability of glycine–sodium nitrate. *Journal of Molecular Structure: THEOCHEM*, *905*(1), 76-80.

[xvi]Cervantes-Navarro, F., &Glossman-Mitnik, D. (2013). Density functional theory study of indigo and its derivatives as photosensitizers for dye-sensitized solar cells. *Journal of Photochemistry and Photobiology A: Chemistry*, *255*, 24-26.

[xvii]Ioniţă, M., Vlăsceanu, G. M., Watzlawek, A. A., Voicu, S. I., Burns, J. S., &Iovu, H. (2017). Graphene and functionalized graphene: Extraordinary prospects for nanobiocomposite materials. *Composites Part B: Engineering*.